EXCELLENT PUBLISHERS

International Journal of Current Research and Academic Review

ISSN: 2347-3215 Volume 3 Number 9 (September-2015) pp. 70-89

www.ijcrar.com

Experimental and Theoretical (FT-IR, FT-Raman) Vibrational Spectroscopic Analysis and Second- and Third-Order NLO Properties of a (2E)-1-(4-bromophenyl)-3-(2-chlorophenyl) prop-2-en-1-one

K.Anitha[1], V.Balachandran[2*] and B.Narayanan[3]

[1]Department of Physics, Bharathidasan University Constituent College, Lalgudi, Tiruchirapalli 621 601, TamilNadu, India
[2]Centre for Research, Department of Physics, A A Government Arts College, Musiri, Tiruchirapalli, 621211, TamilNadu, India
[3]Department of Studies in Chemistry, Mangalore University, Mangalagangotri 574 199, India
Corresponding author

KEYWORDS

Vibrational spectra, MEP surface, HOMO-LUMO, NBO and NHO analysis, Second order NLO, Third orderNLO.

A B S T R A C T

The optimized geometry of (2E)-1-(4-bromophenyl)-3-(2-chlorophenyl) prop-2-en-1-one (BP2CP) has been determined by DFT (B3LYP) and LC-DFT (CAM-B3LYP) method. A detailed vibrational spectral analysis was carried out and the assignments of the observed bands have been proposed on the basis of total energy distribution (TED). Molecular electrostatic potential (MEP) surface was plotted over the geometry to elucidate the reactivity of the molecule. NBO analysis has been performed in order to demonstrate charge transfer or conjugative interaction and delocalization of electron density within the molecule. HOMO–LUMO analysis has been done in order to determine the way the molecule interacts with other species. On the basis of vibrational analysis, other molecular properties such as ionization energy, electron affinity, chemical potential, global hardness and electrophilicity were also calculated. The electronic properties were determined by time-dependent TD-DFT approach. The microscopic second and third-order nonlinear optical (NLO) behaviour of the BP2CP have been computed by both dispersion-free (static) and also frequency-dependent (dynamic) linear polarizabilities (α), first (β) and second order hyperpolarizabilities (γ) using LC-DFT method. From LC-DFT calculation results, the title molecule exhibits high second hyperpolarizabilities, implying microscopic third-order NLO behaviour.

Introduction

Significant interest still exists in the design and development of chalcone derivatives exhibiting large second-order NLO response because of the potential application in telecommunications, optical computing and optical signal processing (Sarojini *et al.*, 2006; Jayarama *et al.*, 2013; Geskin *et al.*, 2003; Aditya Prasad *et al.*, 2015; Anthoni

Praveen Menezes *et al.*, 2014). In the light of wide applications of NLO properties, a large number of materials have been synthesised and their NLO properties have been explored using different techniques like degenerate four-wave mixing, Z-scan and second harmonic generation. Third harmonic generation measurements are particularly interesting since they are strongly related to electronic processes. For the free molecule the dipole and quadrupole moments and the (hyper) polarizabilities values are computed using *ab initio* computation (Maroulis, 1998; Batista *et al.*, 1998; Christiansen *et al.*, 1999). However, experimental determination of the corresponding effective properties in condensed phases is much more difficult and rests on a number of assumptions and approximations whose limitations are difficult to assess. In the present study, it is planned to have FT-IR and FT-Raman spectral measurements, theoretical construction of IR and Raman spectra, variation of the molecular polarizability, hyperpolarizability with the influence of frontier orbital energy, frequency dependent NLO property, molecular electrostatic potential surface, natural bond orbital and natural hybrid orbital analysis, reactivity descriptors and electronic spectra of BP2CP with molecular geometry using DFT and LC-DFT studies.

Experimental details

A 10% solution of KOH was added to a mixture of 4-bromoacetophenone (0.01 mol) and 2-chlorobenzaldehyde (0.01 mol) in 20 ml of ethanol. The resulting mixture was stirred for three hours at room temperature and the precipitate formed was collected by filtration and purified by recrystallization from absolute alcohol (M.P.344-46K). The FT-IR of the BP2CP was measured in the BRUKER IFS 66V spectrometer in the range 4000–400 cm−1. The FT-Raman spectrum of the BP2CP was also recorded in FT-Raman BRUKER RFS 100/S instrument equipped with Nd:YAG laser source operating at 1064 nm wavelength and 150mW power. The spectrum is recorded in the range 3500–100 cm^{-1}. The spectral resolution is ±2 cm^{-1}.

Computational details

All calculations were performed using the Gaussian 09W package (Frisch *et al.*, 2009). The traditional hybrid Becke, three-parameter, Lee–Yang–Parr (B3LYP) exchange correlation functions of the Density Functional Theory (DFT) and the long-range-corrected CAM-B3LYP(LC-DFT) functional was applied using 6-31G (d) basis set. The geometry of BP2CP was fully optimized at the aforementioned levels of theory. The vibrational modes are assigned on the basis of Total Energy Distribution (TED) analysis using Vibrational Energy Distribution Analysis (VEDA) program (Jamroz, 2004). The Raman activities (*si*) calculated by Gaussian 09 program has been converted to relative Raman intensities (*Ii*).

From the basic theory of Raman scattering, Raman activities (is) calculated by Gaussian 09 program has been converted to relative Raman intensities (*Ii*) using the following relationship:

$$I_i = \frac{f(\upsilon_0 - \upsilon_i)^4 s_i}{\upsilon_i[1 - \exp(-hc\upsilon_i)]/kT}$$

where

υ0 is the laser exciting wave number in cm^{-1} (in this work, we have used the excitation wave number = 9398.5cm^{-1}, which corresponds to the wavelength of 1064nm of Nd:YAG laser),

υi is the vibrational wave number of the i^{th} normal mode in cm^{-1},
h, *c*, and *k* are universal constants (is a constant equal to 10^{-12}) and
f is a suitably chosen common normalization factor for all the peak intensities.

The hybrid directionality and bond bending, Natural bond orbital (NBO) analysis were performed on BP2CP by the NBO 3.1 program (Glendening *et al.*, 1998) at the B3LYP/6-31G (d) level as implemented in the Gaussian 09W software package (Dennington *et al.*, 2003). These calculations yielded second-order perturbation energies which have been utilized in locating hydrogen bonding and hyperconjugative interactions. Gauss view 5.1 program (Silverstein *et al.*, 1981) has been considered to get visual animation and also for the verification of the normal modes assignment.

Theoretical NLO calculations

The theoretical computations involve the determination of dispersion-free and frequency-dependent linear polarizability, first and second hyperpolarizability tensor components of the title compound. The components of β are defined as the coefficients in the Taylor series, with expansion of the energy in the external electric field. When the external electric field is weak and homogeneous, this expansion becomes:

$$E(F) = E(0) - \mu_i F_i - \frac{1}{2}\alpha_{ij}F_iF_j - \frac{1}{6}\beta_{ijk}F_iF_jF_k - \frac{1}{24}\gamma_{ijkl}F_iF_jF_kF_l$$

Where, αij, βijk and γijkl are the polarizability, the first hyperpolarizability and second hyperpolarizability tensors, respectively. The subscripts i, j and k label x, y and z components. It is clear that the values of αij, βijk and γijkl can be obtained by differentiating E with respect to F. In this work, the components of the polarizability tensor are obtained as the second-order derivatives of the energy with respect to the Cartesian components (i, j, k = x, y, z) of the electric field, viz.,

$$\alpha_{ij} = \left[d^2E / dF_i dF_j\right]_{F=0}$$

The derivatives are evaluated numerically by using the finite field method and the mean polarizability is calculated from the diagonal elements of the polarizability tensor as,

The static first hyperpolarizability β was calculated by analytical third energy derivatives, which is more efficient and less expensive. The total second-order polarizabilities (β_{tot}) for the studied complexes are defined as:

$$\beta_{tot} = \left(\beta_x^2 + \beta_y^2 + \beta_z^2\right)^{1/2}$$

where β_i is defined as

$$\beta_i = (\beta_{iii} + \beta_{ijj} + \beta_{ikk}) \quad i, j, k = x, y, z.$$

The average second hyperpolarizability γ_{ijkl} can be directly calculated from Gaussian 09[8]. The equation for average second hyperpolrizability is

$$\langle\gamma\rangle = \frac{1}{5}\left[\gamma_{xxxx} + \gamma_{yyyy} + \gamma_{zzzz} + 2\left(\gamma_{xxyy} + \gamma_{xxzz} + \gamma_{yyzz}\right)\right]$$

The tensor elements parallel to long molecular axes or parallel to large transition dipole moments dominate the isotropic values.
The components of linear polarizability, first and second hyperpolarizabilities of the title compound is computed. Since the values of the polarizabilities α, first hyperpolarizability β and second hyperpolarizability γ of Gaussian 09 output are reported in atomic units (a.u.), the calculated values have been converted into electrostatic units (esu) (α: 1 a.u. = 0.1482 X10: 1 a.u. = $8.641X10^{-24}$ e.s.u.; β: 1 a.u. = $8.6393 X 10^{-33}$ e.s.u. and $^{-39}$ e.s.u.).

Result and Discussion

Molecular Geometry

The molecular structure of BP2CP belongs to C1 point group symmetry. The optimized molecular structure of title molecule is obtained from GAUSSIAN 09W (Frisch *et al.,* 2009) and GAUSSVIEW (Dennington *et al.,* 2003) program with the atom numbering scheme given in figure 1. The comparative optimized geometrical parameters (bond lengths and bond angles) calculated by

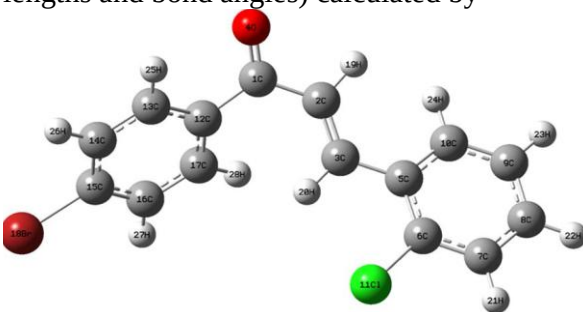

Fig.1 Optimised geometry of (2E)-1-(4-bromophenyl)-3-(2-chlorophenyl)prop-2-en-1-one

B3LYP /6-31G (d) and CAM-B3LYP/6-31G (d) basis sets are listed in table 1. Since the geometry of the molecule obtained by CAM-B3LYP/6-31G (d) method is energetically most stable, hence the theoretical values of this method are taken for correlation and are more reliable.

Vibrational analysis

Experimental FT-IR and FT-Raman spectra and the calculated IR and Raman spectra are shown in figure 2 and 3 for comparative purposes, where the calculated intensity and activity is plotted against the harmonic vibrational frequencies. The experimental wavenumbers are tabulated in table 2 together with the calculated wavenumbers of studied molecule. The resulting vibrational frequencies for the optimized geometry and the proposed vibrational assignments are given in table 2.

Phenyl ring vibrations

Aromatic structures display characteristic C−H stretching vibrations occurring in the region 3100–3000 cm^{-1} (Silverstein *et al.,* 1981; Colthup *et al.,* 1990; Varsanyi, 1974). The BP2CP molecule comprises of two double-substituted phenyl ring. Most of the C−H stretching vibrations are found to be weak which is due to the charge transfer from the hydrogen atom to the carbon atom.

For the C−H stretching vibrations, the band observed at 3061 cm^{-1} in FT-IR and 3080, 3062 and 3020 cm^{-1} in FT-Raman spectrum. These modes are stretching modes as evident from the TED column shown in table 2. The C−H in-plane bending vibration usually occurs in the region 1400–1050 cm^{-1} and the C−H out of plane bending vibrations in the range 1000–675 cm^{-1} (Varsanyi, 1974). In our study the C−H in-plane bending vibrations have been observed at 1468, 1440, 1324, 1177 and 1106 cm^{-1} in FT-IR and 1483, 1472, 1442, 1325, 1290, 1175 and 1161cm^{-1} in FT- Raman and their corresponding theoretical values are quite compatible. The C−H out-of-plane vibrations have been observed at 975, 856, 820, 753 and 711 cm^{-1} in FT-IR and 976, 893, 862, 822 and 762 cm^{-1} in FT-Raman.

The C−C ring stretching vibrations are expected within the region 1650–1200 cm^{-1}. In general, the bands of variable intensity are observed at 1625–1590, 1575–1590, 1470–1540, 1430–1465 and 1280–1380 cm^{-1} from the frequency ranges given by Varsanyi (1969) for the five bands in the region. Most of the ring modes are altered by the substitution to aromatic ring.

The actual positions of these modes are determined not so much by the natural of the substituent but by the form of substitution around the ring system (Bellamy, 1975). The frequency bands at 1599, 1394, 1272, 1213, 1141 and 1059 cm^{-1} in FT-IR and at 1599, 1588, 1575, 1395, 1275, 1204, 1069 and 1040cm^{-1} in FT-Raman spectra were assigned to the C−C stretching vibrations for molecule.

Table.1 A comparison between the optimized geometrical parameters calculated at B3LYP and the long range corrected DFT functional CAM-B3LYP at 6-31G (d) level of theory for (2E)-1-(4-bromophenyl)-3-(2-chlorophenyl) prop-2-en-1-one parameters

Bond length(Å)			BondAngle(°)			Dihedralangle(°)		
Parameter	B3LYP/ 6-31G (d)	CAM-B3LYP/ 6-31G (d)	Parameter	B3LYP/ 6-31G(d)	CAM-B3LYP/ 6-31G (d)	Parameter	B3LYP/ 6-31G (d)	CAM-B3LY P/ 6-31G (d)
C1−C2	1.4836	1.4828	C2−C1−O4	118.5935	118.7181	O4−C1−C2−C3	152.9661	151.7135
C1−O4	1.2282	1.2201	C2−C1−C12	121.5777	121.4516	O4−C1−C2−H19	-18.6477	-20.0455
C1−C12	1.501	1.4973	O4−C1−C12	119.8224	119.8238	C12−C1−C2−33	-26.1134	-27.3516
C2−C3	1.3486	1.3389	C1−C2−3	125.6842	125.2659	C12−C1−C2−H19	162.2727	160.8894
C2−H19	1.0873	1.0863	C1−C2−H19	112.4398	112.8179	C2−C1−C12−C13	152.494	153.0946
C3−C5	1.4669	1.469	C3−C2−H19	121.3359	121.3931	C2−C1−C12−17	-31.3187	-30.5313
C3−H20	1.0851	1.0847	C2−C3−5	125.8232	125.0516	O4−C1−C12−C13	-26.5745	-25.9603
C5−C6	1.4107	1.4015	C2−C3−H20	118.5643	118.9995	O4−C1−C12−C17	149.6128	150.4138
C5−C10	1.4101	1.4015	C5−C3−H20	115.5817	115.923	C1−C2−C3−C5	-175.119	-175.5263
C6−C7	1.394	1.3886	C3−C5−C6	121.7517	121.7461	C1−C2−C3−H20	2.7655	2.5422
C6−Cl11	1.7626	1.7504	C3−C5−C10	121.6586	121.2744	H19−C2−C3−C5	-4.1989	-4.4302
C7−C8	1.3929	1.3874	C6−C5−C10	116.5813	116.9702	H19−C2−C3−H20	173.685	173.6383
C7−H21	1.0846	1.0838	C5−C6−C7	122.0119	121.8498	C2−C3−C5−C6	163.747	157.5949
C8−C9	1.3971	1.391	C5−C6−Cl11	120.8446	120.6582	C2−C3−C5−C10	-17.3421	-23.5474
C8−H22	1.0861	1.0851	C7−C6−Cl11	117.1397	117.4877	H20−C3−C5−C6	-14.1925	-20.5268
C9−C10	1.3889	1.3847	C6−C7−C8	119.7037	119.6906	H20−C3−C5−C10	164.7184	158.3309
C9−H23	1.0859	1.0849	C6−C7−H21	119.4133	119.3564	C3−C5−C6−C7	179.6169	179.6745
C10−H24	1.0853	1.0846	C8−C7−H21	120.8828	120.9529	C3−C5−C6−Cl11	-1.1067	-1.0924
C12−C13	1.4039	1.3968	C7−C8−C9	119.825	119.8475	C10−C5−C6−C7	0.6535	0.7699
C12−C17	1.4027	1.3955	C7−C8−H22	119.6413	119.6632	C10−C5−C6−Cl11	179.93	-179.997
C13−C14	1.3904	1.3851	C9−C8−H22	120.5331	120.4885	C3−C5−C10−C9	-179.647	-179.7237
C13−H25	1.0851	1.0843	C8−C9−C10	119.8817	119.8512	C3−C5−C10−H24	-0.7308	-0.9216
C14−C15	1.3962	1.3903	C8−C9−H23	120.3102	120.3139	C6−C5−C10−C9	-0.6824	-0.8136
C14−H26	1.0845	1.0837	C10−9−H23	119.8063	119.8326	C6−C5−C10−H24	178.2336	177.9885
C15−C16	1.3931	1.3873	C5−C10−C9	121.9927	121.7857	C5−C6−C7−C8	-0.2634	-0.3015
C15−Br18	1.9095	1.8946	C5−C10−H24	118.6532	118.6683	C5−C6−C7−H21	179.5989	179.5624
C16−C17	1.3949	1.3895	C9−C10−H24	119.3453	119.5353	Cl11−C6−C7−C8	-179.565	-179.5578
C16−H27	1.0845	1.0836	C1−C12−C13	117.6064	117.449	Cl11−6−7−H21	0.2969	0.3061
C17−H28	1.0849	1.0839	C1−C12−C17	123.4329	123.3707	C6−C7−C8−C9	-0.1312	-0.1581
			C13−C12−C17	118.8536	119.083	C6−C7−C8−H22	-179.859	-179.8402
			C12−C13−C14	120.9598	120.8248	H21−C7−C8−C9	-179.991	179.9802
			C12−C13−H25	118.5845	118.5512	H21−C7−C8−H22	0.2814	0.2981
			C14−C13−H25	120.4558	120.6238	C7−C8−C9−C10	0.1032	0.1153
			C13−C14−C15	119.0151	119.0684	C7−C8−C9−H23	-179.411	-179.3308
			C13−C14−H26	120.8357	120.8837	H22−C8−C9−C10	179.828	179.7948
			C15−C14−H26	120.1484	120.047	H22−C8−C9−H23	0.3142	0.3487
			C14−C15−C16	121.2769	121.2079	C8−C9−C10−C5	0.3213	0.3893

C14−C15−Br18	119.3234	119.3735	C8−C9−C10−H24	-178.588	-178.4027
C16−C15−Br18	119.399	119.4178	H23−C9−C10−C5	179.8376	179.8381
C15−C16−C17	119.1001	119.1796	H23−C9−C10−H24	0.9288	1.046
C15−C16−H27	120.2432	120.1238	C1−C12−C13−C14	178.2227	178.2791
C17−C16−H27	120.6562	120.6963	C1−C12−C13−H25	-1.7477	-1.587
C12−C17−C16	120.7679	120.613	C17−C12−C13−C14	1.8552	1.7438
C12−C17−H28	120.1612	120.1853	C17−C12−C13−H25	-178.115	-178.1223
C16−C17−H28	119.0455	119.1818	C1−C12−C17−C16	-177.13	-177.2676
			C1−C12−C17−H28	1.019	1.0972
			C13−C12−C17−C16	-0.9877	-0.9496
			C13−C12−17−H28	177.1613	177.4152
			C12−C13−C14−C15	-1.2658	-1.1738
			C12−C13−C14−H26	179.0653	179.1796
			H25−C13−C14−C15	178.704	178.6895
			H25−C13−C14−H26	-0.9649	-0.9571
			C13−C14−C15−C16	-0.2108	-0.2045
			C13−C14−C15−Br18	-179.898	-179.8684
			H26−C14−C15−C16	179.4605	179.4452
			H26−C14−C15−Br18	-0.2268	-0.2187
			C14−C15−C16−17	1.0553	0.9796
			C14−C15−C16−H27	-178.699	-178.8021
			Br18−C15−C16−17	-179.258	-179.3566
			Br18−C15−C16−H27	0.9877	0.8616
			C15−C16−17−C12	-0.4399	-0.3891
			C15−C16−17−H28	-178.609	-178.7702
			H27−C16−17−C12	179.3136	179.3913
			H27−C16−17−H28	1.1442	1.0102

Table.2 Comparison of the experimental (FT-IR and FT-Raman) wavenumbers (cm-1) and theoretical wavenumbers (cm-1) of (2E)-1- (4-bromophenyl)-3-(2-chlorophenyl)prop-2-en-1-one calculated by B3LYP/6- 31G (d) and CAM- B3LYP/6- 31G (d).

No.	Fundamentals (cm^{-1})		Calculated frequencies (cm^{-1}) Unscaled		Scaled		TED (%) among types of internal coordinates
	FT-IR	Raman	FT-6-31G(d)	B3LYP/ 6-31G(d)	CAM-B3LYP/ 6-31G(d)	B3LYP/ 6-31G(d)	CAM-B3LYP/
1			3080	3232	3252	3084	3081	νC14-H26(43), νC13-H25(40), νC16-H27(11)
2				3230	3250	3074	3072	νC16-H27(55), νC17-H28(27)
3	3061		3062	3229	3248	3066	3065	νC7-H21(78), νC8-H22(15)
4				3220	3230	3053	3051	νC10-H24(33), νC3-H20(24), νC9-H23(20)
5	3035			3219	3240	3032	3032	νC3-H20(36), νC10-H24(19), νC9-H23(12)
6			3020	3219	3239	3026	3023	νC13-H25(42), νC14-H26(40), νC3-H20(17)
7				3214	3235	3006	3007	νC17-H28(56), νC3-H20(21), νC16-H27(20)
8				3210	3230	2980	2981	νC8-H22(42), νC10-H24(30), νC9-H23(17)
9				3198	3218	2965	2967	νC9-H23(41), νC8-H22(39), νC2-H19(11)
10	2921			3193	3213	2922	2920	νC2-H19(82), νC10-H24(10)
11			1687	1727	1745	1690	1685	νO4-C1(83), νC2-H19(10)
12	1661		1662	1685	1705	1668	1662	νC2=C3(60), βH20-C3-C2(12)
13	1599		1599	1649	1671	1593	1596	νC6-C7(23), νC9-C10(18), νC7-C8(11)
14				1642	1665	1588	1588	νC13-C14(24), νC16-C17(21)
15			1588	1618	1635	1578	1581	νC8-C9(30), νC5-C10(14), BC6-C7-C8(12)
16			1575	1615	1633	1575	1575	νC14-C15(19), νC15-C16(19), νC12-C17(17), νC12-C13(18)
17			1483	1530	1544	1480	1482	βH26-C14-C13(18), βH27-C16-C17(16), βH28-C16-C17(14), βH25-C13-C14(13)
18	1468		1472	1516	1529	1460	1469	βH24-C10-C9(24), βH21-C7-C8(17), βH23-C9-C8(13), βC7-C8-C9(10)
19	1440		1442	1484	1497	1442	1440	βH22-C8-C9(26), βH23-C9-C8(13), νC6-C7(12), νC5-C10(11), βH21-C7-C8(10)
20	1394		1395	1438	1448	1396	1395	νC13-C14(24), νC16-C17(22), βH27-C16-C17(11),
21				1373	1373	1355	1357	βH20-C3-C2(69), νC2-C3(14)
22	1324		1325	1344	1345	1326	1326	βH26-C14-C13(25), βH26-C14-C13(18), βH25-C13-C14(18), βH27-C16-C17(14), βH28-C16-C17(11)
23				1339	1333	1310	1311	νC1-C12(14), βH24-C10-C9(11), νC1-C2(10), βH28-C16-C17(11)
24				1335	1328	1307	1306	βH19-C2-C3(55), βH21-C7-C8(25)
25			1290	1318	1325	1298	1296	βH24-C10-C9(23), νC3-C5(14), νC9-C10(10),
26	1272		1275	1316	1302	1274	1274	νC15-C16(21), νC12-C17(20), νC14-C15(19), νC12-C13(13), νC13-C14(10)
27	1213			1284	1279	1215	1214	νC6-C7(24), νC5-C10(17)
28			1204	1240	1245	1207	1206	νC9-C10(19), βH21-C7-C8(15) νC3-C5(11),
29	1177		1175	1212	1216	1176	1176	βH25-C13-C14(19), βH27-C16-C17(19), βH28-C16-C17(19), βH26-C14-C13(16),
30			1161	1198	1198	1166	1160	βH21-C7-C8(29), βH23-C9-C8(27), βH21-C7-C8(13), νC8-C9(10)
31	1141			1154	1162	1140	1142	νC7-C8(23), βH21-C7-C8(18), βH24-C10-C9(12)
32	1106			1140	1144	1106	1105	βH25-C13-C14(20), νC16-C17(19), νC13-C14(14), βH26-C14-C13(14), βH27-C16-C17(16), βH28-C16-C17(11)
33	1068		1069	1102	1113	1063	1062	νC1-C2(19), νC12-C13(14)
34	1059			1088	1097	1058	1058	νC15-C16(22), νC14-C15(27), νC13-

							C14(10)
35		1040	1079	1085	1040	1041	νC8-C9(24), βH21-C7-C8(18), νC7-C8(12), βH23-C9-C8(10), βC6-C7-C8(11)
36		1021	1054	1065	1022	1020	βC6-C7-C8(26), νC8-C9(13), νCl11-C6(13)
37		1012	1038	1052	1010	1014	γC3-C2-C5-H20(66), τH19-C2-C3-C5(25)
38	1005		1026	1035	1003	1006	βC13-C12-C17(29), βC14-C15-C16(28), νC12-C17(14), νC12-C13(13)
39	975	976	994	1019	975	976	γC13-C12-C14-H25(58), τH26-C14-C13-C12(31)
40			990	1018	930	933	τH22-C8-C9-H23(65), τH24-C10-C5-C3(12)
41			987	1013	900	902	τH27-C16-C17-H28(83), τH27-C16-C17-C12(14)
42		893	956	983	890	893	τH21-C7-C8-H22(62), τH24-C10-C5-C3(12)
43		862	909	932	855	860	τH19-C2-C3-C5(48), γC3-C2-C5-H20(18), γO4-C2-C12-C1(14)
44	856		882	903	850	856	τH24-C10-C5-C3(12), τH22-C8-C9-H23(19),τH21-C7-C6-C5(16)
45	820	822	871	888	820	821	τH26-C14-C13-C12(22), τH27-C16-C17-C12(14), γC13-C12-C14-H25(11)
46			859	880	810	813	τH27-C16-C17-C12(60),τH26-C14-C13-C12(19), γC13-C12-C14-H25(13)
47	800		856	868	800	802	βC7-C8-C9(17), νC3-C5(13), νC5-C10(11)
48		762	785	800	756	760	τH21-C7-C6-C5(34)
49	753		767	780	750	753	τH21-C7-C6-C5(16), τH21-C7-C8-H22(15), τH24-C10-C5-C3(13), τC5-C6-C7-C8(12)
50		733	759	776	731	730	τC12-C13-C14-C15(13), τC12-C17-C16-C15(13), βC14-C15-C16(12), γO4-C2-C12-C1(10)
51	711		729	749	712	710	τC5-C6-C7-C8(31), τC5-C10-C9-C8(20), τC12-C13-C14-C15(13), τC12-C17-C16-C15(13)
52		700	711	719	692	700	βC8-C9-C10(28), νCl11-C6(23)
53		677	680	697	673	675	γO4-C2-C12-C1(32), τC12-C13-C14-C15(11), τC12-C17-C16-C15(11)
54		626	657	665	621	625	βC2-C1-C4(15), βC8-C9-C10(10)
55		587	642	648	585	586	βC15-C16-C17(66)
56	581		620	626	578	580	βC2-C1-C4(13), βC7-C8-C9(12), βC5-C10-C9(11)
57	532	535	558	567	531	533	βC2-C1-C12(19), τC7-C8-C9-C10(14)
58	508		522	536	508	508	τC7-C8-C9-C10(40), τC8-C7-C6-Cl11(10)
59		487	487	497	481	486	τC14-C13-C12-C17(46), βC3-C5-C10(10)
60			468	478	460	461	τC5-C10-C9-C8(28),τC5-C6-C7-C8(15)
61			457	469	443	447	τC5-C10-C9-C8(16), βC3-C5-C10(10)
62			428	442	420	422	τC12-C17-C16-C15(36), τC12-C13-C14-C15(33)
63		416	419	426	415	416	βC5-C6-Cl11(22), βC2-C1-C4(21), νBr18-C15(10)
64		385	403	407	380	380	νCl11-C6(35), βC6-C7-C8(14)
65			318	327	310	309	τC1-C2-C3-C5(15), τC3-C5-C10-C9(11)
66		275	297	305	272	275	βC14-C15-Br18(32), βC1-C12-C13(14)
67		263	267	276	260	261	τC17-C16-C15-Br18(13), τC3-C5-C10-C9(12), τC8-C7-C6-Cl11(11), νBr18-C15(10), τC1-C12-C13-C14(10)
68			248	254	215	217	νBr18-C15(16), βC5-C6-Cl11(11)
69		185	239	248	180	185	βC5-C6-Cl11(23), τC17-C16-C15-Br18(17)
70			180	196	171	170	τC8-C7-C6-Cl11(41), τC3-C2-C1-C12(22)
71		165	167	177	162	163	τC3-C2-C1-C12(23), τC2-C3-C5-C10(10)
72			153	168	140	143	βC1-C12-C13(26), βC14-C15-Br18(25), τC3-C2-C1-C12(12)

73		114	128	122	121	
74	108	90	108	108	110	τC3-C5-C10-C9(20), βC2-C1-C12(10) τC2-C1-C12-C17(35), τC1-C2-C3-C5(15),βC3-C5-C10(10), τC3-C5-C10-C9(10)
75	83	77	92	79	80	τC17-C16-C15-Br18(26), τC1-C12-C1
76		50	80	50	51	C14(22), βC2-C3-C5(11), βC1-C2-C3(1
77		28	43	41	40	τC2-C1-C12-C17(45), τC1-C2-C3-C5(19),τC2-C3-C5-C10(14) 3-0)
78		10	37	36	35	τC2-C3-C5-C10(23), τC1-C2-C3-C5(2 βC2-C1-C12(17),βC1-C2-C3(13) τC2-C3-C5-C10(30), τC1-C12-C13-C14(16), τC3-C2-C1-C12(12), βC1-C2-C3(10) 0), 0),

ν; Stretching, β; in-plane bending, γ; out-of-plane bending, τ; torsion. [a] Total energy distribution.

The C−C−C in-plane bending vibrations are observed at 1005, 800, 581 and 532 cm^{-1} in FT-IR and 1021, 700, 626, 587, 535, 416 and 385 cm^{-1} in FT-Raman. The C−C−C out-of-plane bending vibrations are observed at 711, 508 in FT-IR and 733, 535, 487, 108 and 83cm^{-1} in FT-Raman.

The theoretical computed C−C−C in plane and out-of-plane bending vibrations by the CAM-B3LYP/6-31G (d) shows good agreement with the recorded spectral data and presented in table 2. All these calculated values are in good agreement with the experimental data. The remainder of the observed and calculated wavenumbers and their assignments of the compound are shown in table 2.

Ethylenic bridge group (−CH=CH−) vibrations

The vibrations of the ethylenic bridge are highly sensitive to the degree of charge transfer between the donor and the acceptor groups, hence such stretching modes are of particular interest for spectroscopists (Ying *et al.*, 2004). The sharp intense band in infrared spectrum at 1661cm−1and in Raman spectrum at 1662 cm−1 is assigned to C2=C3 stretching mode. The aliphatic C−H stretching bands are expected between 3050 and 3000 cm−1. The C−H stretching modes are predicted experimentally at 3035 and 2921 cm−1 in FT-IR spectrum. The bands corresponding to in-plane and out-of-plane deformations are observed as expected, in the regions 1500–1000 cm−1 and 1000–750 cm−1, respectively (Amit Kumar *et al.*, 2014). The C2=C3 torsion mixed with the out of plane bending of C−H is observed in the Raman spectrum at 1012cm^{-1}. The intensity and band position correlate with the calculated value are shown in table 2.

C=O vibrations

The C=O stretching, vibration band can be easily identified from the IR and Raman spectra, because of the degree of conjugation, strength and polarizations. The characteristic infrared absorption frequencies of carbonyl group have been extensively investigated. The C=O stretching vibration band can be easily identified in the IR and Raman spectrum as due to high degree of conjugation, the strength and polarization are increased. The carbon– oxygen double bond is formed by π–π bonding between carbon and oxygen. Because of the different electronegativities of carbon and oxygen atoms, the bonding electrons are not equally distributed between the two atoms. The carbonyl stretching vibrations in ketones are expected in the region 1715– 1680 cm^{-1} (Bellamy, 1975). In our case, the C=O stretching bands are observed at 1687cm^{-1} in FT-Raman spectrum. Theoretically computed wavenumbers are in the range of 1690 and 1685 cm^{-1}.

Fig.2 Experimental and calculated FT-IR spectra of (2E)-1-(4-bromophenyl)-3-(2-chlorophenyl)prop-2-en-1-one

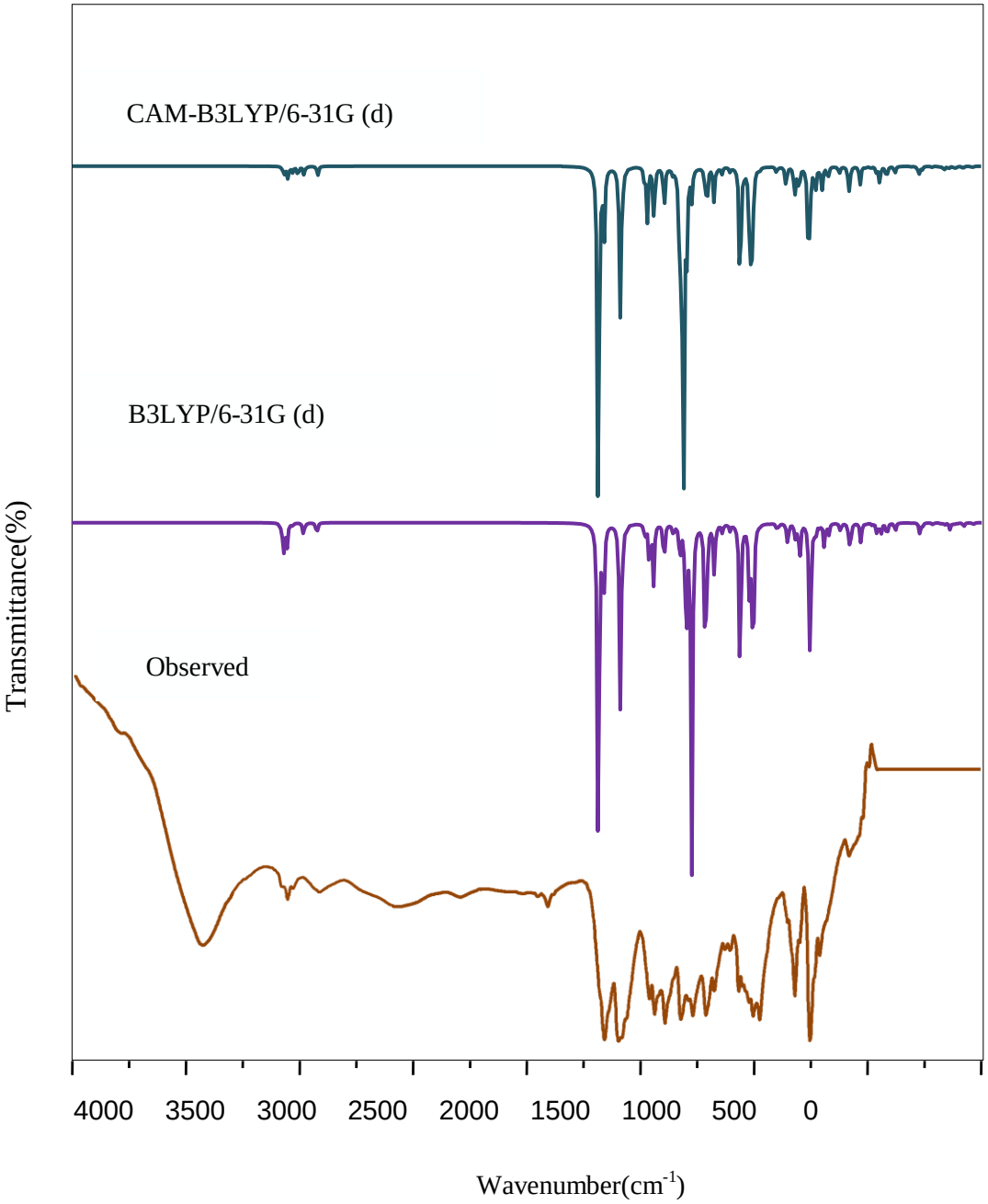

Fig.3 Experimental and calculated FT-Raman spectra of (2E)-1-(4-bromophenyl)-3-(2-chlorophenyl)prop-2-en-1-one

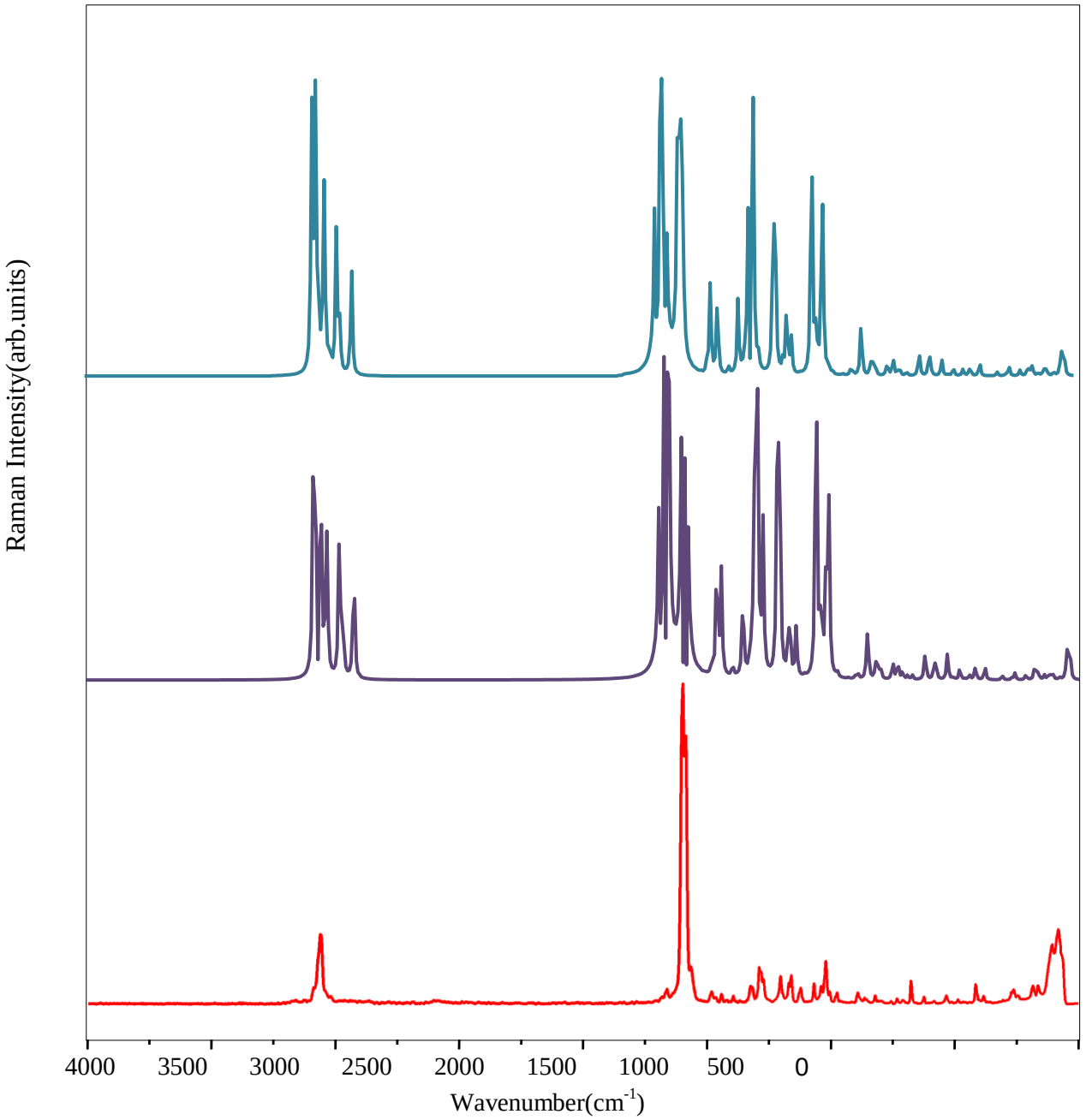

C−Cl and C−Br vibrations

Chlorine and bromine atoms directly attached to the aromatic ring give rise bands.

Mooney *et al.* (1963, 1964) assigned vibrations of C−Cl, Br, and I in the wavenumber range of 129–480 cm^{-1}. The C−Cl stretching vibrations give generally strong bands in the region 710–505 cm^{-1}. For simple organic chlorine compounds, C−Cl absorptions are in the region 750–700 cm^{-1}. For the title compound, the band observed at 700 cm^{-1} in the FT-Raman spectrum is assigned as the C−Cl stretching

mode. The deformation bands of C−Cl are also identified. The C−Cl deformation bands are reported at 185 cm^{-1} in FT-Raman spectrum. The assignments of C-Br stretching and deformational modes have been made through comparison with TED calculations. The vibrations belonging to the bond between the ring and Bromine atom is important as mixing of vibrations is possible due to the presence of heavy atom (Chiu *et al.*, 1979; Najiya *et al.*, 2014; Samdal *et al.*, 1997). Bromine compounds normally absorb in the region of 650–450 cm^{-1} due to the C–Br stretching vibrations (Mooney, 1964; Arthur *et al.*, 2009). In the present study, the medium strong band due to C-Br stretching vibration is observed at 416 cm^{-1} in FT-Raman spectrum. The in-plane and out-of-plane C–Br bending vibrational assignments are listed in table 2.

NHO and NBO analysis

According to the simple bond orbital picture, a NBO is defined as an orbital formed from NHOs. Therefore, for a localized σ- bond between atoms A and B, the NBO is defined as:

$$\sigma AB = cA\ hA + cB\ hB$$

where hA and hB are the natural hybrids centered on atoms A and B and cA and cB are the polarization coefficients for atoms A and B. The direction of each hybrid is specified in terms of the spherical polar (θ) and azimuthal (φ) angles from the nucleus as well as the deviation angle Dev from the line of centers between the bonded nuclei. For more general spλdμ hybrids, the hybrid direction is determined numerically to correspond to the maximum angular amplitude and then compared with the direction of the line of centers between the two nuclei to determine the bending of the bond, expressed as the deviation angle (Dev, in degrees) between these two directions. The angular properties of the natural hybrid orbitals are very much influenced by the type of substituent that causes conjugative effect or steric effect. In table 3, the bending angles of different bonds are expressed as the angle of deviation from the direction of the line joining the two nuclei centers. Similar deviations are shown by carbon NHOs of bonds C5–C6, C7–C8, C9–C10, C13–C14 and C15–C16 constituting the phenyl rings from the line of C5–C6, C7–C8, C9–C10, C13–C14 and C15– C16 nuclear centers (90.0°). Carbon NHO of σ is more bent away from the line of C2–C3 centers by 7.4° due to steric repulsion effect around these centers, whereas the carbon NHO is bent only by an angle of 7° as a result of lying in the strong charge transfer path. A little lower bending effect (1.4°) is also noticed at C1–C12 bond due to vicinal bonded atoms around these centers (Threshold for printing *Dev* in Gaussian output is 1.0°).

NBO theory allows the assignment of the hybridization of atomic lone pairs and of the atoms involved in bond orbitals. These are important data in spectral interpretation since the frequency ordering is related to the bond hybrid composition. The NBO analysis allows us to estimate the energy of the molecule with same geometry but in the absence of electronic delocalization. Moreover, only the steric and electrostatic interactions through the Lewis are taken into account. NBO analysis has been performed on BP2CP with NBO 3.1 program (Glendening *et al.*, 1998) in order to elucidate intermolecular hydrogen bonding, intermolecular charge transfer (ICT), rehybridization and delocalization of electron density. A short outline of the NBO segments used and their structural meaning is presented below. The most important interactions between 'filled' (donor) Lewis-type NBOs and 'empty' (acceptor) non-Lewis NBOs are reported in table 4. In addition, the occupancy of natural bonds and lone pairs, and the percentage of p-character calculated by NBO analysis are also given. The stabilization energy ΔE_{ij} associated with delocalization is estimated using the second-order perturbation theory as:

$$E(2) = \Delta E_{ij} = q_i \varepsilon - \varepsilon$$

where q_i is the donor orbital occupancy, εi and εj are diagonal elements and *F (i, j)* is the off- diagonal NBO Fock matrix element. The NBO bond polarization and hybridization changes were associated with formation of the compound. In NBO analysis, large *E(2)* value shows the intensive interaction between electron-donors and electron-acceptors and greater the extent of conjugation of the whole system, the possible intensive interactions are given in table 4. As the filled NBOs get close together a steric repulsion occurs as a consequence of the Pauli's exclusion principle giving rise to a destabilizing energy *E(2)*. Such a high destabilizing energy estimated for the molecule is in agreement with the manifestation of molecular strain as evidenced by the molecular data.

The hyperconjugative interaction between π (C15 – C16) and π*(C12 – C17) is 203.66 kcal/mol. There occurs a strong intramolecular hyperconjugative interaction of the π*(C5 – C6) with the π * (C7–C8) orbital which leads to the stabilization of 183.48 kcal/mol. This enhanced π * (C5–C6) NBO further conjugates with π * (C9 –C10) resulting in an enormous E (2) energy of 157.10 kcal/mol. These increasing interaction energies are due to strong delocalization leading to stabilization of the molecule.

Table.3 NHO directionality and ''bond bending'' (deviations from line of nuclear centers) of H-bonded NBOs in (2E)-1-(4-bromophenyl)-3-(2-chlorophenyl)prop-2-en-1-one calculated at B3LYP/6-31+G (d) level

NBO	Line of Centers		Hybrid 1			Hybrid 2		
	Θ	*Φ*	*Θ*	*Φ*	*Dev*	*Θ*	*Φ*	*Dev*
BD (1) C 1 - C 2	101.3	340.5	101.8	342.3	1.9	81	161.6	2.5
BD (2) C 1 - O 4	72	97.1	17.9	292	89.4	19	291.3	89.5
BD (1) C 1 - C 12	95.3	216.8	95.1	215.4	1.4	85	34.9	1.9
BD (1) C 2 - C 3	86.6	287.9	93.8	286.6	7.4	100.4	108.8	7
BD (2) C 2 - C 3	86.6	287.9	11.4	2.8	83.7	15.2	53.8	84.5
BD (1) C 5 - C 6	72.5	287.8	71.6	283.7	4	106.1	113.3	5.5
BD (2) C 5 - C 6	72.5	287.8	26.8	55.1	89.5	27.8	56.3	89.4
BD (1) C 5 - C 10	116.7	39.3	116.5	41.9	2.3	63.1	217.2	1.8
BD (1) C 6 - C 7	97.5	340.7	95.4	336.4	4.8	80.8	164.2	3.8
BD (1) C 7 - C 8	116.6	41.2	116.2	37.2	3.7	63	225.1	3.5
BD (2) C 7 - C 8	116.6	41.2	152.6	236	90	152.6	235.7	90
BD (1) C 8 - C 9	108.4	106.4	109.6	102.4	3.9	72.8	290.3	3.9
BD (1) C 9 - C 10	82.2	161.3	83.7	158.2	3.4	98.9	343.9	2.9
BD (2) C 9 - C 10	82.2	161.3	27.9	56.1	90.1	151.7	236.4	90.1
BD (1) C 12 - C 13	55.1	166	54.1	164.3	1.7	124	348.4	2.1
BD (1) C 12 - C 17	132	265.4	130.9	270.6	4	47.2	80.8	3.5
BD (2) C 12 - C 17	132	265.4	44.6	299.6	92.5	130.9	118	88
BD (1) C 13 - C 14	94.1	213.3	91.6	211.1	3.3	83.2	35.7	3.6
BD (2) C 13 - C 14	94.1	213.3	45.8	299.5	90.1	133.7	119.2	89.8
BD (1) C 14 - C 15	132	267.1	129.8	261.9	4.5	45.6	94.7	6
BD (1) C 15 - C 16	126.6	345.5	129.3	338.8	6	55.5	170.4	4.5
BD (2) C 15 - C 16	126.6	345.5	133.1	119	89.7	132.4	118.9	89.7

Dev. – Deviation ; *Θ* – Polar angle; *Φ* – Azimuthal angle.

HOMO- LUMO and Reactive escriptors

The Eigen values of HOMO (π- donor) and LUMO (π- acceptor) and their energy gap reflect the chemical activity of the molecules. Recently, the energy gap between HOMO and LUMO has been used to prove the microscopic NLO activity from intra-molecular charge transfer (ICT). Also, energies of HOMO and LUMO are used for the determination of global reactivity descriptors. It is important that Ionization potential (*I*), Electron affinity (*A*), Electrophilicity (ω), Chemical potential (μ), Electronegativity (χ), Hardness (η) and Softness (*S*) be put into a MO framework.

We focus on the HOMO and LUMO energies in order to determine the interesting molecular/atomic properties and chemical quantities. In simple molecular orbital theory approaches, the HOMO energy is related to the ionization potential *(I)* and the LUMO energy has been used to estimate the electron affinity *(A)* respectively by the following relations:
$I = -E_{HOMO}$ and $A = -E_{LUMO}$
The chemical potential of the molecule is $(\phi) = -(I + A)/2$. The absolute hardness of the molecule is $(\eta) = (I - A)/2$.
The softness is the inverse of the hardness $(S) = 1/\eta$.

Table.4 Selected second order perturbation energies of the (2E)-1-(4-bromophenyl)-3-(2-chlorophenyl) prop-2-en-1-one were calculated using B3LYP/ 6-31+G (d) chemistry level

Donor	ED(i)(e)	Energy(i) (a.u)	Acceptor (j)	ED(j)(e)	Energy(j) (a.u)	[a]E(2) (kcal/mol)	E(j)-(i) (arb.units)	F(i,j) (arb.units)
π (C5 – C6)	1.64760	-0.27726	π*(C7 – C8)	0.31813	0.01715	19.10	0.29	0.068
π(C7 – C8)	1.65722	-0.26605	π*(C5 – C6)	0.43523	0.00082	20.96	0.27	0.068
π(C7 – C8)	1.65722	-0.26605	π*(C9 – C10)	0.29864	0.02048	18.56	0.29	0.066
π(C9 – C10)	1.67431	-0.26560	π*(C5 – C6)	0.43523	0.00082	19.95	0.27	0.067
π(C9 – C10)	1.67431	-0.26560	π*(C7 – C8)	0.31813	0.01715	20.61	0.28	0.068
π(C12 – C17)	1.64015	-0.25874	π*(C13 – C14)	0.28495	0.02682	19.94	0.29	0.069
π(C12 – C17)	1.64015	-0.25874	π*(C15 – C16)	0.37877	0.00675	20.97	0.27	0.067
π(C13 – C14)	1.65642	-0.25920	π*(C12 – C17)	0.36416	0.02287	18.74	0.28	0.065
π(C13 – C14)	1.65642	-0.25920	π*(C15 – C16)	0.37877	0.00675	22.01	0.27	0.069
π(C15 – C16)	1.67217	-0.27524	π*(C12 – C17)	0.36416	0.02287	19.36	0.3	0.068
LP (2) O4	1.89049	-0.25471	σ*(C1 – C12)	0.06722	0.43152	19.60	0.69	0.105
π*(C1 – O4)	0.17983	0.01453	π*(C2 – C3)	0.09761	0.03766	34.30	0.02	0.068
π*(C5 – C6)	0.43523	0.00082	π*(C2 – C3)	0.29	0.03766	40.17	0.04	0.067
π*(C5 – C6)	0.43523	0.00082	π*(C7 – C8)	0.31813	0.01715	183.48	0.02	0.08
π*(C5 – C6)	1.64760	0.00082	π*(C9 – C10)	0.29864	0.02048	157.10	0.02	0.082
π(C15 – C16)	1.67217	-0.27524	π*(C12 – C17)	0.36416	0.02287	203.66	0.02	0.084
π(C15 – C16)	1.67217	-0.27524	π*(C13 – C14)	0.28495	0.02682	127.06	0.02	0.078

ED: Electron density
[a]E(2) means energy of hyper conjugative interaction (stabilization energy).
[b]Energy difference between donor and acceptor i and j NBO orbitals.
[c]F(i, j) is the Fock matrix element between i and j NBO orbitals.

The electronegativity of the molecule is $(\chi) = (I + A)/2$.
The electrophilicity index of the molecule is $(\omega) = \phi 2/2\eta$.

This value assesses energy decreasing due to maximal electron flow between donor (HOMO) and acceptor (LUMO) shown in figure 4. The calculated values of the global reactivity descriptors for the title molecule are collected in table 5. In terms of chemical hardness, if a molecule has a large HOMO–LUMO gap, it is hard. Conversely, if the HOMO–LUMO gap is small, it is soft. One can also relate molecular stability to hardness, which means that the molecule with smaller HOMO–LUMO gap is more reactive.

Molecular electrostatic potential (MEP)

The graphical representation of the molecular electrostatic potential surface (MEP or ESP), as described by Kollman and Singh (Singh and Kollman, 1984) is a series of values representing the evaluation of the interaction energy between a positively charged (proton) probe and points on a solvent accessible surface as defined by Connolly (Connolly, 1983). As implemented within the Gauss View version 5.1 program (Dennington *et al.*, 2003), areas of high electron density, representing a strong attraction between the proton and the points on the molecular surface, have the brightest red colour and areas of the lowest electron density have deep blue to indigo colour indicating the regions of maximum repulsion. The maximum values of ESP show that the ring carbons and hydrogens are acidic, exhibit greater positive potential as ~0.032a.u. With the addition of electron withdrawing group there is a area of negative potential at the polar carbonyl group C1=O4 consistent with having a greater electron density than ring carbon atoms, exhibits negative potential as~ −0.048a.u. In contrast, regions close to the other two polar atoms – bromine Br18 (~ −0.014a.u), and chlorine Cl11 (~ −0.011a.u) – show regions of mildly negative potential. The addition of electron withdrawing groups produces a large increase in positive potential at the center of the ring (Fig. 5).

Fig.4 HOMO & LUMO plot of (2E)-1-(4-bromophenyl)-3-(2-chlorophenyl)prop-2-en-1-one

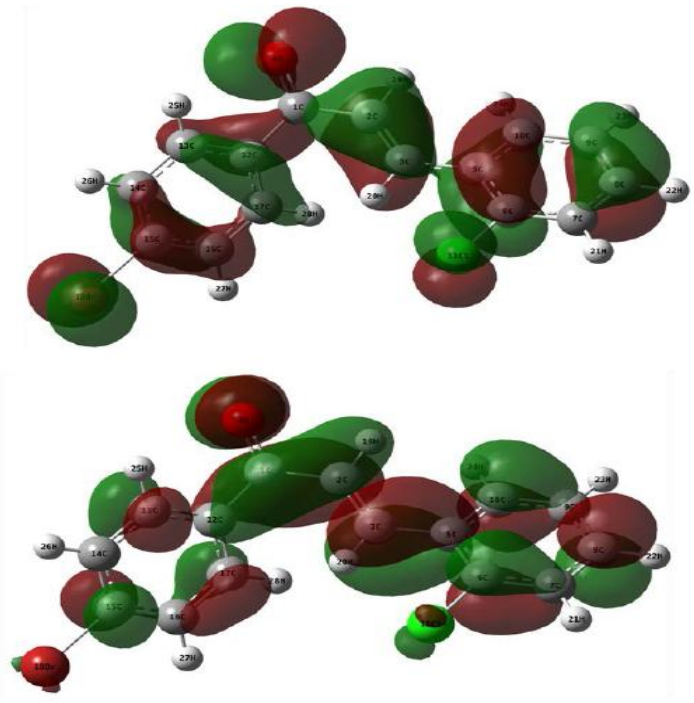

Table.5 The HOMO - LUMO energy gap ionisation potential, Electron affinity, Chemical Hardness, Electronegativity, Softness, Chemical potential, Global electrophilicity index values of (2E)-1-(4-bromophenyl)-3-(2-chlorophenyl)prop-2-en-1-one at the B3LYP /6-31G(d) and CAM-B3LYP/6-31G(d) level

Parameters	B3LYP/ 6-31G(d)	CAM-B3LYP/ 6-31G(d)
E_{HOMO}(ev)	-6.669	-8.064
E_{LUMO}(ev)	-2.199	-1.174
$E_{HOMO} - E_{LUMO}$ gap(ev)	4.4706	6.889
Ionisation potential(I, ev)	-6.669	-3.4448
Electron affinity(E, ev)	-2.198	-4.619
Chemical Hardness(η, ev)	-2.235	-0.290
Electronegativity(χ, ev)	-4.434	4.619
Softness(S,ev^{-1})	-0.447	-0.290
Chemical potential(φ, ev)	4.434	4.619
Global electrophilicity index(ω)	-4.398	-3.097

The variance in ESP surfaces shows an increase in the intensity of this localized positive potential in the molecule becomes more electron-deficient. Thus, the ESP surface measurements identify two complementary regions within the compound. A region of zero potential envelopes the π-system of the benzene rings, leaving a more electrophilic region in the plane of the hydrogen atoms.

Static and dynamic NLO property

The determination and analysis of the NLO properties of molecular systems with theoretical methods have greatly progressed during the past years. Actually, to accurately compute NLO properties of rather great molecular systems like metal complexes and polymers, there are well-tested computational codes. In particular, an accurate analysis of the NLO behaviour of those great molecules leads to the definition of high-order hyperpolarizability values as well as third-order. Once conceived, the idea can be first pursued by theoretical means, and promising results would justify experimental efforts to obtain the envisioned compounds synthetically as well. One could determine the hyperpolarizability tensors of molecules using a suitable computational approach. These tensors describe the response of molecules to an external electric field. At the molecular level, the NLO properties are determined by their dynamic hyperpolarizabilities. Garza et al (Garza *et al.,* 2013) observed that the methods with long-range corrections (‘‘LC’’ and ‘‘ω’’ methods) perform roughly equally among themselves, but improve the accuracy significantly over standard hybrids. LC-DFT method with CAM-B3LYP functional is a procedure used here to find out approximate values and can be a means of understanding both static and dynamic hyperpolarizabilities of BP2CP. In this study, in addition to the static linear polarizabilities α(0; 0), first β(0;0,0) and second γ(0; 0, 0, 0), hyperpolarizabilities, the following processes for dynamic (hyper) polarizabilities have been considered: frequency-dependent linear polarizabilities

α(-ω; ω), SHG β(-2 ω; ω, ω, ω), THG γ(-3 ω; ω, ω, ω), Some significant calculated magnitudes of the static and frequency-dependent linear polarizabilities, first and second hyperpolarizabilities are shown in tables 6 and 7, respectively.

Generally, the molecular hyperpolarizabilities, β (−2ω; ω, ω), have been measured in a fundamental incident wavelength which has a second harmonic far enough from the absorption bands to avoid the over measure of β values due to resonance effects. Hence, two near resonant wavelength of ω=0.0428 a.u. (1064 nm) and ω=0.0340 a.u. (1340 nm), one non-resonant wavelength of ω=0.0239 a.u. (1907 nm) are adopted to compute the frequency dependence. As shown in table 6, the magnitude of the frequency-dependent first hyper-polarizability increases with the increasing frequency (Anitha and Balachandran, 2015). The values of β(−2ω;ω,ω) in the BP2CP are larger than that of β(−ω;ω,0), and both of the β(−2ω;ω,ω) and β(−ω;ω,0) values are larger than the corresponding static βtot values. Thus, β(−2ω; ω, ω) exhibits the largest frequency dispersion. < γ > values depend on a number of factors, which include extent of π-electron conjugation, the dimensionality of the molecules and the nature of substituents. The role of phenyl rings in determining the NLO response in π conjugate chalcone derivatives, since it can act either as the donor or the bridging moiety of the donor-(π conjugate-bridge)-acceptor system. However, in presence of strong donor–acceptor substituents, the phenyl rings mostly acts as a bridge and is mainly responsible for the dispersion- free and frequency-dependent second hyperpolarizabilities with non-zero values as microscopic NLO response of the investigated molecule.

Fig.5 The molecular electrostatic potential surface of (2E)-1-(4-bromophenyl)-3-(2-chlorophenyl)prop-2-en-1-one

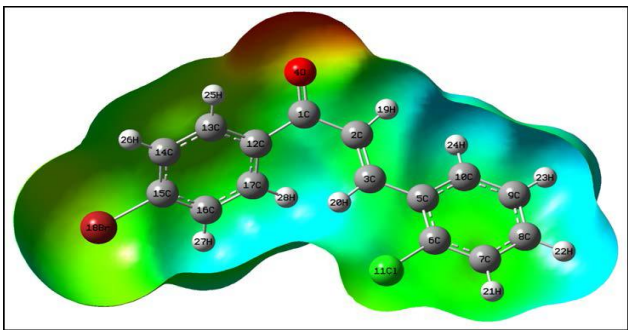

Table.6 The static linear polarizability (α), static anisotropic polarizability (Δα), dipole moment (μ), static first-order hyperpolarizability(β) and static second-order hyperpolarizability(γ) values of (2E)-1-(4-bromophenyl)-3-(2-chlorophenyl)prop-2-en-1-one in Gas phase.

Methods	CAM-B3LYP/6-31G(d)
α x 10^{-23} (esu)	2.669
$\Delta\alpha$ x 10^{-23} (esu)	2.353
μ(Debye)	3.851
β x 10^{-30} esu	8.033
γ x 10^{-34} esu	5.072

Table.7 The dynamic linear polarizability (α ×10−23esu), dynamic anisotropic polarizability (Δα ×10−23esu), dynamic first-order hyperpolarizability (β × 10-30 esu) and dynamic second-order hyperpolarizability (γ× 10-34 esu) values of (2E)-1-(4-bromophenyl)-3-(2-chlorophenyl) prop-2-en-1-one in Gas phase.

Parameters	ω=0.0239 a.u	ω=0.0340 a.u	ω=0.0428 a.u
α (-ω, ω)	2.686	2.703	2.724
Δα (-ω, ω)	2.377	2.402	2.433
β(-ω,ω,0)	8.353	8.706	9.145
β(-2ω,ω,ω,)	9.059	10.357	12.281
γ(-ω,ω,0)	5.294	5.540	5.849
γ(-3ω,ω,ω,)	5.794	6.723	8.131

Electronic properties

In the UV–Vis region with high extinction coefficients, all molecules allow strong π–π* and σ–σ* transition (Silverstein *et al.*, 1991). In an attempt to understand the nature of electronic transitions in terms of their energies and oscillator strengths, in this study CAM-B3LYP (Yanai *et al.*, 2004) hybrid functional including long range corrected hybrids are used. CAM-B3LYP is a long-range corrected functional that uses a Coulomb attenuating method to combine the hybrid B3LYP method with a long-range correction by introducing two extra parameters, instead of the single parameter used by Tian *et al.* (2010). The calculated excitation energies, oscillator strength (f) and wavelength (λ) and spectral assignments are given in table 8. The major contributions of the transitions are designated with the aid of Gausssum2.2 program (O'Boyle *et al.*, 2008). Due to the Frank– Condon principle, the maximum absorption peak (λmax) in an UV–visible spectrum corresponds to vertical excitation. The strong transitions at 3.65 eV (340 nm) in gas phase, is assigned to n–π* transition. The theoretical UV–Vis spectrum of BP2CP is shown in figurew 6. In view of calculated absorption spectra, the maximum absorption wavelength corresponds to the electronic transition from the HOMO-3 to LUMO with 57% contribution. The other wavelength, excitation energies, oscillator strength and calculated counterparts with major contributions can be seen in table 8.

Table.8 Theoretical electronic absorption spectra of (2E)-1-(4-bromophenyl)-3-(2-chlorophenyl) prop-2-en-1-one (absorption wavelength λ (nm), excitation energies, E (eV) and oscillator strengths (f) using TD–DFT/CAM-B3LYP/6-31G (d) methods in gas phase.

No.	*E* (ev))	*λ*(nm)	*f*	[a]Major contribution
1	3.6452265	340.1276655	0.0021	H-3→L (57%)
2	4.526133	273.9297334	0.6696	H→L (71%)
3	4.8563354	255.3041135	0.0815	H-2→L (63%)

[a] H – HOMO, L – LUMO.

Fig.6 Calculated electronic spectrum of (2E)-1-(4-bromophenyl)-3-(2-chlorophenyl) prop-2-en-1-one

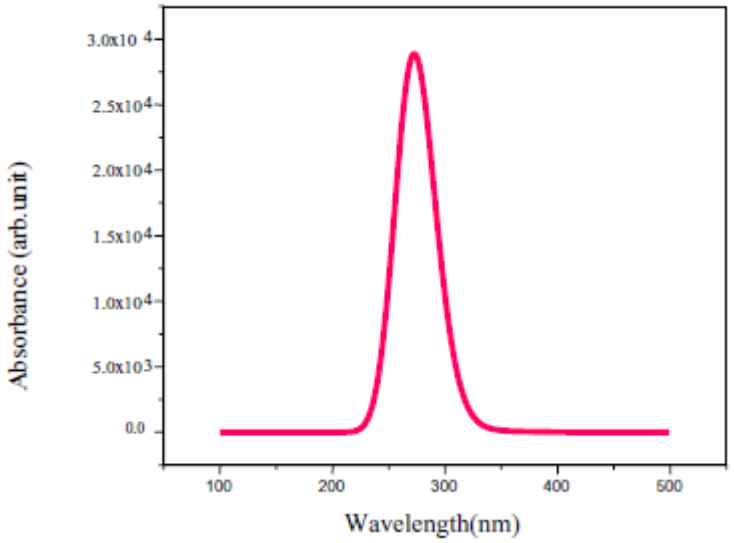

Conclusion

FT-IR and FT-Raman spectra of (2E)-1-(4-bromophenyl)-3-(2-chlorophenyl) prop-2-en-1-one are studied both experimentally and theoretically. The computations were performed at DFT and LC-DFT levels of theory to get the optimized geometry and vibrational wave numbers of the normal modes of the title compound. The HOMO and LUMO analysis is used to determine the charge transfer within the molecule. The stability of the molecule arising from hyper-conjugative interaction and charge delocalization has been analyzed using NBO analysis. From the MEP it is evident that the negative region are mainly localized over the C=O group. The electronic properties are also calculated. The energies of important MOs and the λmax of the compound are also evaluated from TD-CAM-B3LYP method with 6-31G (d) basis set. The first order β (SHG) and second order γ (THG) hyperpolarizabilities obtained using the CAM-B3LYP method for the title compound demonstrate promising practical applications in nonlinear optics. We conclude that the title compound and its derivatives are attractive objects for future studies of nonlinear optical properties.

References

Aditya Prasad, A., Muthu, K., Meenatchi, V., Rajasekar, M., Agilandeshwari, R., Meena, K., Vijila Manonmoni, J., Meenakshisundaram, S.P. 2015. *Spectrochimica Acta part A: Mol. Biomol. Spectrosc.*, 140: 311–327.

Amit Kumar, Vipin Deval, Poonam Tandon, Archana Gupta, E. Deepak D'silva, 2014. *Spectrochim. Acta part A*, 130: 41−53.

Anitha, K., Balachandran, V. 2015. *Spectrochimica Acta Part A: Mol. Biomol. Spectrosc.*, 146: 66–79.

Anthoni Praveen Menezes, A., Jayarama, Seik Weng, Ng, *J. Crystal Growth*, 402: 130–137.

Arthur, J., Plante, L., Stidham, D.H. 2009. *Spectrochim. Acta A*, 74: 808–818.

Batista, E.R., Xantheas, S.S., Jo´ nsson, H. 1998. *J. Chem. Phys.*, 109: 4546–4551.

Bellamy, L.J. 1975. The infrared spectra of complex molecules, Vols. 1 and 2, Chapmann & Hall, London.

Bellamy, L.J. 1975. The infrared spectra of complex molecules. Capman and Hall, London.

Chiu, N.S., Ewbank, J.D., Askari, M., Schafer, L. 1979. *J. Mol. Struct.*, 54: 185–190.

Christiansen, O., Gauss, J., Stanton, J.F. 1999. *Chem. Phys. Lett.*, 305: 147–155.

Colthup, N.B., Daly, L.H., Wiberley, S.E. 1990. Introduction to Infrared and Raman Spectroscopy, Academic Press, New York.

Connolly, M.L. 1983. *Science,* 221: 709–713.

Dennington, R.I., Keith, T., Millam, J., Eppinnett, K., Hovell, W. 2003. Gauss View Version 3.0.

Frisch, M.J., Trucks, G.W., *et al.* 2009. Gaussian 09: Revision A. 02; Gaussian. Inc., Wallingford, CT.

Garza, A.J., Scuseria, G.E., Khan, S.B., Asiri, A.M. 2013. *Chem. Phys. Lett.*, 575: 122–125.

Geskin, V.M., Lambert, C., Bredas, J.L. 2003. *J. Am. Chem. Soc.*, 125: 15651–15658.

Glendening, E.D., Reed, A.E., Carpenter, J.E., Weinhold, F. 1998. NBO Version 3.1, TCI, University of Wisconsin, Madison.

Jamroz, M.H. 2004. Vibrational energy distribution analysis, VEDA 4 Computer Program, Poland.

Jayarama, A., Ravindra, H.J., Anthoni Praveen Menezes, S.M. Dharmaprakash, Seik Weng, Ng. 2013. *J. Mol. Structure,* 1051: 285–291.

Maroulis, G. 1998. *Chem. Phys. Lett.*, 289: 403–411.

Mooney, E.F. 1963. *Spectrochim. Acta*, 19: 877–887.

Mooney, E.F. 1964. *Spectrochim. Acta*, 20(6): 1021–1025.

Mooney, E.F. 1964. *Spectrochim. Acta*, 20: 1021–1032.

Najiya, A., Yohannan Panicker, C., Sapnakumari, M., Narayana, B., Sarojini, B.K., Van Alsenoy, C. 2014. *Spectrochimica Acta Part A: Mol. Biomol. Spectroscopy*, 133: 526–533.

O'Boyle, N.M., Tenderholt, A.L., Langner, K.M. 2008. *J. Comp. Chem.*, 29: 839−845.

Samdal, S., Strand, T.G., Tafipolsky, M.A., Vilkov, L.V., Popik, M.V., Volden, H.V. 1997. *J. Mol. Struct.*, 435: 89–95.

Sarojini, B.K., Narayana, B., Ashalatha, B.V., Indira, J., Lobo, K.G. 2006. *J. Crystal Growth*, 295: 54–59.

Silverstein, M., Basseler, G.C., Morill, C. 1981. Spectrometric identification of organic compounds, Wiley, New York.

Silverstein, R.M., Bassler, G.C., Morrill, T.C. 1991. Spectrometric identification of organic compounds, John Wiley, Chichester.

Singh, U.C., Kollman, P.A. 1984. *J. Comput. Chem.*, 5: 129−145.

Tian, B., Eriksson, E.S.E., Eriksson, L.A. *J. Chem. Theory Comput.*, 6: 2086−2094.

Varsanyi, G. 1969. Vibrational spectra of benzene derivatives, Academic Press, NewYork.

Varsanyi, G. 1974. Assignments for vibrational spectra of 700 benzene derivatives, Adam Hilger, London.

Yanai, T., Tew, D.P., Handy, N.C. 2004. *Chem. Phys. Lett.*, 393: 51−57.

Ying Li, Zhi-Ru Li, Di Wu, Rui-Yan Li, Xi-Yun Hao, Chia-Chung Sun, 2004. *J. Phys. Chem. B*, 108: 3145–3148.